

Hidden microscopic life of the moving contact line of a waterlike liquid

Juan Carlos Fernández-Toledano ^{*}, Terence D. Blake , and Joël De Coninck
*Laboratory of Surface and Interfacial Physics (LPSI), Department of Physics,
University of Mons, Mons, Belgium*

Matej Kanduč 
Jožef Stefan Institute, SI-1000 Ljubljana, Slovenia

 (Received 27 February 2020; accepted 22 September 2020;
published 16 October 2020)

We have used large-scale molecular dynamics (MD) simulations to investigate the contact-line friction of a waterlike liquid interface moving across a flat solid surface. The dynamic contact angle θ_D has been measured as a function of contact-line speed U_{cl} using two configurations: a liquid drop spreading spontaneously on a stationary solid surface and a liquid bridge in Couette flow between two solid surfaces moving in opposite directions at a range of steady speeds. The wettability of the solid surface was systematically varied to give a range of equilibrium contact angles θ^0 from 38 to 126 deg. The coefficient of contact-line friction ζ was determined from the expression $\zeta U_{cl} = \gamma_L(\cos \theta^0 - \cos \theta_D)$, where γ_L is the surface tension of the liquid. This simple linear equation, which maybe derived from the molecular-kinetic theory (MKT) of dynamic wetting, is predicted to apply at sufficiently low values of U_{cl} . In addition, we have applied a Langevin formalism to extract the coefficients of contact-line friction directly from the equilibrium fluctuations of the contact line, without any additional theoretical interpretation or model. Both approaches yield the same values for the coefficient within the probable uncertainty, confirming that this intriguing property is determined only by equilibrium properties. Overall, our results show that contact-line friction is a real phenomenon, intrinsic to wetting and applicable to real liquids such as water. Thus, models of dynamic wetting that ignore it are incomplete. From a practical perspective, the concept of a simple linear relationship between surface tension driving force and contact-line velocity may provide a useful simplification in many areas such as nanotechnology where contact-line speeds can be low. Another finding from our study is that slip between water and a molecularly flat, partially wetted solid surface is minimal, with slip lengths of little more than the diameter of a water molecule for equilibrium contact angles of 90 deg or less. Furthermore, we have confirmed a mechanistic link between the coefficients of slip and contact-line friction, specifically $\beta = \zeta/\delta$, where δ is the thickness of the contact line when viewed at the molecular scale. Thus measurements of the dynamic contact angle or contact-line fluctuations may potentially be used to predict slip and vice versa.

DOI: [10.1103/PhysRevFluids.5.104004](https://doi.org/10.1103/PhysRevFluids.5.104004)

I. INTRODUCTION

From both scientific and technological perspectives, the wetting of solids by liquids is an extreme example of a multiscale problem, both spatially and temporally. Thus while the boundary

^{*}carlos.toledano@umons.ac.be

conditions for continuum descriptions of wetting are set at the molecular level, i.e., the nanoscale, the consequences may be felt at all scales up to kilometers, as, for example, in the transport of groundwater in aquifers or the distribution of oil and gas in petroleum reservoirs. Similarly, while the molecular events that determine wetting may have a duration of nanoseconds or less, their consequences in the above examples may occur over geological time. In laboratory experiments, we can make observations at the micrometre scale and, through modeling, describe events at as large a scale as we wish, but bridging the gap down to the critical molecular level is much more difficult, though some progress has been made [1–4]. It is for this reason that wetting research turned to simulations, such as molecular dynamics (MD), to establish the physics that determines the local, microscopic dynamic contact angle and associated properties such as contact-line friction [5–9] and slip [10–12].

Because of computational limits and the need, nevertheless, to generate systems large enough to demonstrate realistic macroscopic behavior, i.e., consistent with continuum models, MD studies of equilibrium systems, spreading drops, capillary flow, forced wetting, etc. were restricted initially to rather simple molecular systems: usually Lennard-Jones (L-J) fluids on molecularly smooth or only marginally rough solid substrates. The simulated liquids typically exhibited rather low surface tensions and viscosities, which raised questions as to their generality. However, with the advent of faster codes and greatly improved computational resources, it has become possible to carry out simulations of wetting using more realistic models of liquids and solids [13,14]. This brings simulation closer to experiment and can lead not only to improvements in our theoretical understanding, but also to simulations that can be applied with more confidence to practical issues, including condensation [15], superhydrophobic surfaces [16], drop impact [17], and closely related problems such as flow through membranes [18] and deicing [19].

In this work we have applied these improved computational methods to determine the contact-line friction of a waterlike liquid at ambient temperature in contact with a molecularly smooth solid substrate having a range of wettabilities. Two different approaches have been taken to interpret the results based on our earlier MD studies with L-J liquids [20–23].

The first approach involves measuring the velocity dependence of the dynamic contact angle in two configurations. In configuration 1, a liquid drop is brought into contact with a solid surface and spreads towards its equilibrium state. During spreading, the contact angle relaxes from a nominal 180 deg at contact towards its equilibrium value as the velocity of the leading edge of the drop, the contact line, decreases to zero. We record the position of the contact line and the contact angle as a function of time, from which we can determine the dependence of the contact angle on contact-line velocity [7,20] and so extract the contact-line friction ζ using the concepts of the molecular-kinetic theory of dynamic wetting (the MKT) [24,25].

In configuration 2, we study a liquid bridge between moving plates in steady-state Couette flow at a range of plate velocities [21]. This generates a corresponding range of dynamic advancing and receding contact angles θ_{adv} and θ_{rec} , respectively, from which we may also obtain ζ . Snapshots of typical drop and liquid-bridge configurations are shown in Fig. 1. Details of the methods are given in Sec. III.

The second approach also exploits the liquid-bridge configuration. When the plates are stationary, we recover the equilibrium contact angle and can follow the thermal fluctuations of the four contact lines of the liquid bridge about their equilibrium positions. This enables us to open a new line of attack using statistical theory to model the fluctuations as an overdamped Langevin oscillator to extract ζ directly from an equilibrium system [22,23]. In Sec. V we compare the contact-line frictions obtained in each case to demonstrate the value of the concept to our understanding of dynamic wetting. We also discuss the link between contact-line friction and slip and the implication of our findings to hydrodynamic treatments of dynamic wetting and related concepts such as the generalized Navier boundary condition (GNBC).

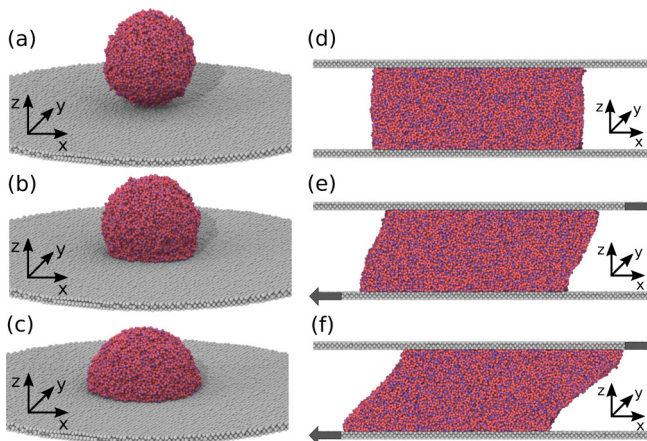


FIG. 1. (a), (b), and (c): Snapshots of drop spreading simulations at successive times $t = 0, 0.09,$ and 1.1 ns, respectively. (d), (e), and (f): Snapshots of capillary bridge simulations for plate velocities $U_{\text{plate}} = 0, 16,$ and 24 m/s, respectively. All correspond to a solid-liquid interaction coupling $C_{SL} = 9$.

II. THEORY

A. Contact-line friction

A theoretical model relating the microscopic dynamic contact angle θ_D to the steady velocity of the contact line U_{cl} was first proposed by Blake and Haynes in 1969 [24]. Their equations have been developed further in the intervening years [25,26] and have proved effective in modeling dynamic contact angle behavior found in both experimental studies and MD simulations, e.g., [9,25,27,28]. The basic idea is that the leading edge of the liquid (L) moves stochastically by way of individual molecular displacements between discrete interaction sites on the surface of the solid (S). The driving force for this process is the localized shear-stress induced by surface tension when the contact angle deviates from its equilibrium value θ^0 . Per unit length of the contact line, this force is $F_{cl} = \gamma_L(\cos \theta^0 - \cos \theta_D)$, where γ_L is the surface tension of the liquid. The force acts across the width of the three-phase contact zone (TPZ), i.e., the contact line viewed at the molecular scale, and is dissipated irreversibly in overcoming the activation energy barriers associated with each molecular displacement. The principle equation linking θ_D to U_{cl} is

$$U_{cl} = 2\kappa^0\lambda \sinh\left(\frac{\gamma_L(\cos \theta^0 - \cos \theta_D)}{2nk_B T}\right), \quad (1)$$

where κ^0 and λ are, respectively, the characteristic (i.e., most probable) frequency and length of molecular displacements, n is the number of interaction sites per unit area, k_B is the Boltzmann constant, and T the absolute temperature. If the interaction sites are distributed uniformly and molecules move only between adjacent sites, then $\lambda \approx 1/\sqrt{n}$.

As yet, no simulation of dynamic wetting has unequivocally demonstrated the nonlinearity predicted by Eq. (1), so the focus has been on using its linear approximation to determine the so-called contact-line friction [7]. If the argument of the sinh function is small, i.e., at low velocities near equilibrium or for systems in which the ratio $\gamma_L\lambda^2/k_B T$ is intrinsically low, Eq. (1) reduces to

$$\zeta U_{cl} = \gamma_L(\cos \theta^0 - \cos \theta_D), \quad (2)$$

where $\zeta = k_B T/\kappa^0\lambda^3$ is the coefficient of contact-line friction per unit length of the contact line (Pa s). Therefore, once we have θ_D as a function of U_{cl} , we can select the region of sufficiently low contact-line velocities and fit Eq. (2) to determine the coefficient ζ . This is straightforward for steady contact-line velocities, as in our forced wetting simulations, but to apply the same

procedure to spreading drops we must assume that the collective behavior of the contact line follows some succession of local equilibrium states. The observable world being the result of microscopic interactions, this is tantamount to assuming that $U_{cl} < \kappa^0 \lambda$. However, in practice, we measure average values of U_{cl} and θ_D over a contact-line length $\Delta L \gg \lambda$ and a small but finite time interval $\Delta t \gg \tau^0 = 1/\kappa^0$, so this is not a critical limitation. Averaging is intrinsic to experimental determinations of U_{cl} and θ_D , where we are limited by the time and spatial resolution of our imaging device, but it is also true in simulations, where we follow an averaging protocol to minimize noise.

One complication is the possibility of slip between the liquid and the solid during forced wetting, as in the simulations of a liquid bridge between moving plates [21]. Slip is especially prevalent in simulations of L-J fluids on molecularly smooth solid surfaces [29]. There must always be slip at the contact line, otherwise the contact line could not move [30], but slip at the general solid-liquid interface has another effect: it reduces the effective contact-line velocity. If the apparent contact-line velocity is U_{cl}^{app} , then $U_{cl} = U_{cl}^{\text{app}} - U_{\text{slip}}$, where U_{slip} is the slip velocity. Thus Eq. (2) becomes

$$U_{cl} = U_{cl}^{\text{app}} - U_{\text{slip}} = \frac{\gamma_L}{\zeta} (\cos \theta^0 - \cos \theta_D). \quad (3)$$

Slip does not appear to be a problem in simulations of spreading drops, where the flow patterns are entirely different [21].

B. Langevin formalism

In a recent study [22] we used MD simulations of a simple L-J liquid bridge at equilibrium between two solid plates to show that the intrinsic thermal fluctuations of contact-line position $x_{cl}(t)$ with time may be modeled as an overdamped, one-dimensional Langevin oscillator [31,32] of stiffness k , confined about its equilibrium position x_{cl}^0 by an harmonic potential $V = 0.5k(x_{cl}(t) - x_{cl}^0)^2$ and damped by contact-line friction ζ . This leads directly to

$$\zeta \frac{dx_{cl}(t)}{dt} = -\hat{k}(x_{cl}(t) - x_{cl}^0) + \hat{f}, \quad (4)$$

where $\hat{k} = k/L_y$, and L_y is the length of the contact line used to compute $x_{cl}(t)$. The random force \hat{f} is due to the fluctuations of the contact angle $\theta(t)$ about its equilibrium value θ^0 , which induce a very fast variation in the capillary force $\gamma_L(\cos \theta^0 - \cos \theta(t))$. This force is uncorrelated at very short times, has a zero mean $\langle \hat{f} \rangle_t = 0$, and must satisfy $\langle \hat{f}(t)\hat{f}(t_0) \rangle_{t_0} = 2\zeta k_B T \delta(t - t_0)/L_y$. Here, $\delta(t - t_0)$ is the classic Dirac delta distribution. In consequence, there is a relation between \hat{k} and the temporal evolution of the signal $x_{cl}(t)$ which allows one to compute \hat{k} :

$$\hat{k} = \frac{k_B T}{\sigma^2 L_y}, \quad (5)$$

where σ^2 is the variance of the contact-line position $\langle x_{cl}^2(t_0) \rangle_{t_0}$. For a given system, the product of the variance and the contact-line length, $\sigma^2 L_y$, is independent of L_y . Furthermore, the contact-line friction ζ may be determined from the time decay of the self-correlation function $\langle x_{cl}(t_0 + t)x_{cl}(t_0) \rangle_{t_0}$:

$$\langle x_{cl}(t_0 + t)x_{cl}(t_0) \rangle_{t_0} = \sigma^2 \exp\left(-\frac{\hat{k}}{\zeta}t\right) = \sigma^2 \exp(-bt). \quad (6)$$

The parameter $b = \hat{k}/\zeta$ determines the rate of decay. The larger the value of b , the more rapidly the system becomes uncorrelated. Once we know both $\sigma^2 L_y$ and b from an analysis of the fluctuations, we can compute the contact-line friction as

$$\zeta = \frac{k_B T}{b\sigma^2 L_y}. \quad (7)$$

TABLE I. Average equilibrium contact angles θ^0 for the drop and liquid-bridge configurations and coefficients of contact-line friction computed from simulations of spontaneous spreading ζ_{SP} , moving plates ζ_{MP} , and fluctuations ζ_F at each solid-liquid coupling C_{SL} studied. Also shown are the slip lengths L_{slip} and the parameters $\sigma^2 L_y$ and b obtained from the contact-line fluctuations.

C_{SL}	θ^0 (deg)	ζ_{SP} (mPa s)	ζ_{MP} (mPa s)	ζ_F (mPa s)	L_{slip} (nm)	$\sigma^2 L_y$ (nm ³)	b (1/ns)
5	125.8 \pm 2.5	0.35 \pm 0.16	0.33 \pm 0.18	0.62 \pm 0.16	2.06 \pm 0.15	0.29 \pm 0.04	21.3 \pm 4.1
8	101.3 \pm 2.8	0.87 \pm 0.23	1.15 \pm 0.25	1.00 \pm 0.23	0.79 \pm 0.17	0.21 \pm 0.02	17.2 \pm 3.0
9	91.0 \pm 1.9	1.19 \pm 0.26	1.34 \pm 0.31	1.24 \pm 0.24	0.59 \pm 0.23	0.26 \pm 0.03	13.1 \pm 1.2
11	72.4 \pm 2.1	1.50 \pm 0.32	1.88 \pm 0.32	1.75 \pm 0.26	0.54 \pm 0.22	0.25 \pm 0.01	9.3 \pm 1.4
14	37.5 \pm 3.3	2.14 \pm 0.41	1.86 \pm 0.44	2.03 \pm 0.49	0.41 \pm 0.21	0.26 \pm 0.04	7.6 \pm 1.3

Thus we can use *equilibrium* measurements to determine a key parameter of *dynamic* wetting. This is a major advantage, since it is quite independent of any theoretical explanation of the velocity dependence of the dynamic contact angle.

III. MD SIMULATIONS

A. The model system

The MD simulations are performed within the LAMMPS software package [33], which has been widely used to study wetting phenomena at the nanoscale [8,13,34–36]. The Newton equations are integrated with a time step of 2 fs and the neighbor lists updated. In all cases, the temperature is set to 300 K and controlled with the Nose-Hoover thermostat [37].

We use the SPC/E model for water [38] that utilizes a tetrahedral representation of the water molecule having an oxygen-hydrogen (OH) distance of 0.1 nm, with a L-J site located on the oxygen atom and positive ($q_H = 0.4236e$) and negative ($q_O = -0.8472e$) charges located on the hydrogen and oxygen atoms, respectively. Coulomb interactions are treated using the particle-mesh-Ewald method with a 1.2-nm real-space cutoff and a precision of 10^{-4} relative to the force between unit point charges at a distance of 1 Å. The H-O-H bond angle of water (109.47°) is fixed using the SHAKE algorithm implemented in LAMMPS [39]. In the SPC/E model, no L-J interactions are considered between oxygen and hydrogen, whereas the oxygen-oxygen interaction parameter is set at $\epsilon_{OO} = 0.650$ kJ/mol for the depth of the potential well and $a_{OO} = 0.3165$ nm for the diameter. The cutoff for the L-J interaction is at 1.2 nm. Standard masses of 16 and 1 g/mol have been used for the O and H atoms, respectively.

The solid surfaces comprise carbonlike atoms with a mass of 12 g/mol, which interact through a L-J potential characterized by a diameter $a_{SS} = 0.35$ nm and a potential well depth $\epsilon_{SS} = 0.3867$ kJ/mol. The solid atoms are arranged in a three-layer, rectangular, fcc lattice with lattice parameter $2^{1/6}a_{SS} = 0.393$ nm (the equilibrium distance of the solid-solid L-J interaction). The solid atoms are allowed to vibrate thermally around their initial positions according to a harmonic potential: $V_h(r) = 1000\epsilon_{SS}|\mathbf{r} - \mathbf{r}_0|^2$, where \mathbf{r} is the instantaneous position of a given atom and \mathbf{r}_0 its initial position.

The L-J potential is also used to describe the interaction between the oxygen atoms of the water and the solid atoms, with parameters $\epsilon_{SO} = 0.2C_{SL}$ kcal/mol, $a_{SO} = 0.3581$ nm, and a $2.5a_{SO}$ cutoff [13]. The nondimensional coupling parameter C_{SL} enables us to adjust the relative affinities between the water molecules and the solid atoms, which in addition to influencing the dynamics of wetting, determines the equilibrium contact angle. The values of C_{SL} studied range from 5 to 14, corresponding to equilibrium contact angles from 126 to 38 deg, respectively, as shown in Table I. The couplings are much higher than those used for L-J fluids. This is necessary to ensure the contact angles span the partial wetting regime.

In a preliminary simulation, we compute the surface tension of a plane liquid slab comprising 41,535 water molecules placed between two vacuum regions with surfaces normal to the z axis and periodic boundary conditions enforced in the x and y directions. At its equilibrium density, the slab has dimensions $L_x = L_y = 10.6$ nm and a thickness $H = 17$ nm, much greater than the range of influence of the free surfaces. The surface tension is obtained from the relationship $\gamma_L = 0.5L_z(\langle P_N \rangle - \langle P_T \rangle)$, where $\langle P_N \rangle$ and $\langle P_T \rangle$ are the pressure tensors perpendicular and tangential to the liquid-vacuum interface [37,40]. Averaged over 5 ns, we obtain $\gamma_L = 56.8 \pm 3.2$ mN/m. From the same simulation, we measure the liquid density $\rho_L = 0.97 \pm 0.03$ g/cm³ and the liquid-vacuum interfacial thickness $d = 0.39 \pm 0.02$ nm. These values are consistent with previous MD simulations using the SPC/E model for water [41]. The self-diffusion coefficient $D = (2.90 \pm 0.06) \times 10^{-9}$ m²/s is computed from the mean-squared displacement using the Einstein relation in an independent simulation of liquid molecules in a cubic box of side $L = 7.1$ nm, with periodic boundary conditions in all directions and the same values of ρ_L and T . The value of the diffusion coefficient is similar to that reported by Tazi *et al.* [42] for the same parameters, where the viscosity η_L is given as 0.64 ± 0.02 mPa s.

B. Drop spreading simulations

For the substrate, we use a 40-nm-diameter solid disk constructed as described above and located in the x - y plane. At the start, the liquid droplet comprises a cube of 13,634 water molecules located 20 nm above the center of the plate (the z direction) to avoid any interaction with the solid. We then run the simulation with periodic boundary conditions in all directions for 2 ns, which is sufficient to reach equilibrium, as characterized by constant energy and a spherical liquid drop with a radius of 4.7 nm. After equilibration, we translate the drop towards the plate until the minimum distance between the centers of the solid and liquid atoms is 0.5 nm and run the simulation for an additional 2 ns, which is sufficient for the drop to spread and attain its equilibrium contact angle.

To determine the contact angle and radius at any instant, we must first locate the L-V interface. Details of the method have been given in previous publications [7,20]. In brief, we divide the drop into horizontal layers 0.1 nm in thickness. We calculate the density of atoms as a function of the radial distance from the midpoint of each layer as determined by symmetry. The L-V interface for each layer is located at the distance at which the density decays to 50% of its central value. To measure the contact angle, we find the best circular fit to the measured interfacial profile. The circular fit is then extrapolated to the position of the first layer of liquid atoms in contact with the solid. The tangent to the circle at this point gives the contact angle and the base radius, as in a real experiment. An example of contact angle measurement is shown in Fig. 2(a).

A limitation of this method is that for a short time after the drop contacts the solid, a large part of the bottom surface of the drop is within range of solid-liquid interactions. For our droplets of radius 4.7 nm, this amounts to some 17% at time zero. The localized attraction means that the S-L interface is initially being created over a much larger area than that assumed by the simple geometric model of a plate intersecting a sphere. A similar effect has been reported for the early stages of the coalescence of liquid drops [43]. Creation of an equilibrium S-L interface takes a very short but finite time [20], and its extent at any instant can be established by measuring the density of the first layer of liquid in contact with the solid and comparing it with the density at long times. If we do this, we find that at very short times (less than about 0.01 ns), the radius of equilibrium contact is larger than that obtained by fitting a circle to the drop. This impacts the accuracy of the measured values of both the contact-line velocity and the dynamic contact angle. However, by the time the angle and speed have fallen to values at which there is a clear linear dependence between F_{cl} and U_{cl} , the difference between the two measures of the base radius is within the noise of the simulations; hence Eq. (2) may safely be applied to determine ζ .

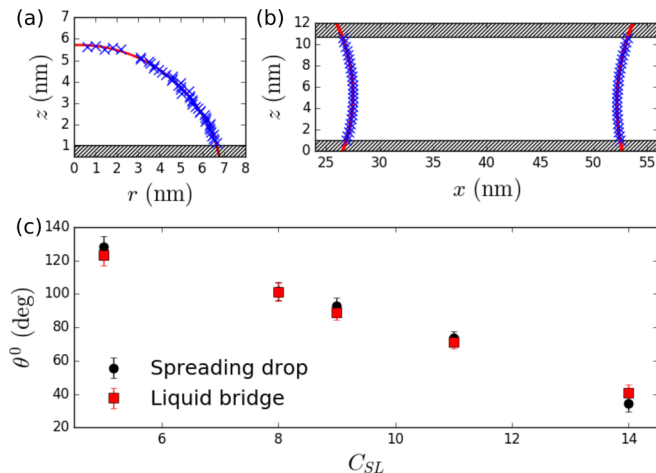


FIG. 2. (a) Drop profile and circular fit at equilibrium for $C_{SL} = 11$. (b) Bridge profile and circular fits at equilibrium for $C_{SL} = 11$. (c) Comparison of the equilibrium contact angles obtained for the spontaneous spreading and liquid-bridge simulations.

C. Capillary bridge simulations

The liquid bridge is constructed from 55,255 liquid molecules at equilibrium density between two parallel solid plates separated by a distance $H = 10.34$ nm. The overall dimensions of the simulation box are $(L_x, L_y, L_z) = (79.6, 6.6, 13.7)$ nm, and we impose periodic boundary conditions in the x and y directions. At the start of the simulation, the liquid is equilibrated between the plates for 1.5 ns, which is sufficient to achieve a stable configuration. To perform our analysis of the contact-line fluctuations at equilibrium, we restart the simulation for additional 2×10^6 time steps (4 ns).

We determine the equilibrium contact angles θ^0 by first averaging 2×10^3 configurations at intervals of 10^3 time steps (0.002 ns). To locate the front and back menisci, we compute the local density in the x - z plane and define the interface at the point where the density falls to 50% of the bulk density, as before. The menisci have constant curvature when averaged over time; hence θ^0 may be found by fitting an arc of a circle to the meniscus profile and measuring its tangent at the solid, as illustrated in Fig. 2(b).

For the dynamic studies we move the two solid plates in opposite directions parallel to the x axis at a constant speed U_{plate} for 2×10^6 time steps (4 ns) until a steady state is achieved. This is indicated by steady advancing and receding contact angles. The simulation is then continued for an additional 1.5×10^6 time steps (3 ns), and the positions of the particles are saved every 10^3 time steps (0.0015 ns) for 1.5×10^3 configurations. These are then averaged to measure the dynamic contact angles using the same method as at equilibrium but fitting the upper and lower parts of the menisci with separate circular arcs. Depending on the S-L coupling, plate speeds from 1 to 35 m/s were used. The speed range is limited by the size of the simulation box and the stability of the liquid bridge. At sufficiently high speeds the liquid bridge may rupture or the receding menisci cross the lateral boundaries of the simulation box.

IV. RESULTS

A. Drop spreading

The evolution of the apparent radius of contact and the dynamic contact angle during the spreading of a water droplet are shown in Fig. 3 for all five solid-liquid couplings, $C_{SL} = 5, 8, 9, 11$, and 14, that we studied. Figures 1(a)–1(c) show successive snapshots during the spreading process

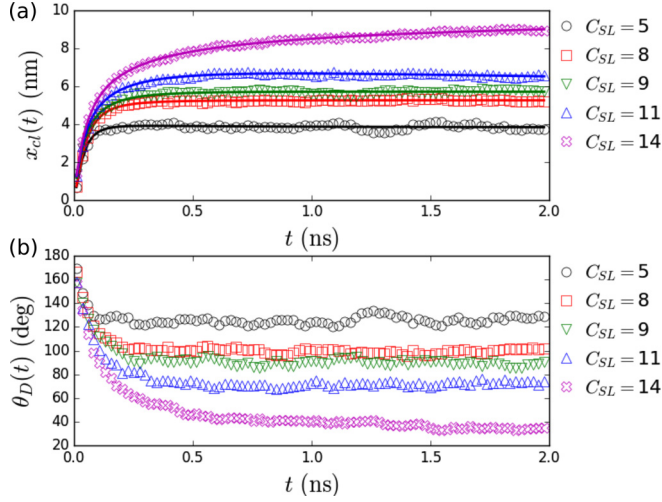


FIG. 3. Evolution of (a) radius of contact $x_{cl}(t)$ and (b) dynamic contact angle $\theta_D(t)$ for spreading drop simulations with five different solid-liquid affinities C_{SL} .

for $C_{SL} = 9$. In each case the dynamic contact angle starts from a nominal 180 deg and relaxes to its equilibrium value after a period that increases with the coupling. Equilibrium is assumed to be achieved once no further change is detectable within the noise of the simulation. Table I lists the average values of the equilibrium contact angles for the drop and the liquid-bridge configurations at each coupling. The individual values are also plotted in Fig. 2(c). There is good agreement between the results from the two sources.

To determine the contact-line frictions, we first compute the contact-line velocity using the method described by de Ruijter *et al.* [7]. We fit the time evolution of the radius of contact with a ratio of polynomials and extract the contact-line velocity by simple differentiation. Figure 4

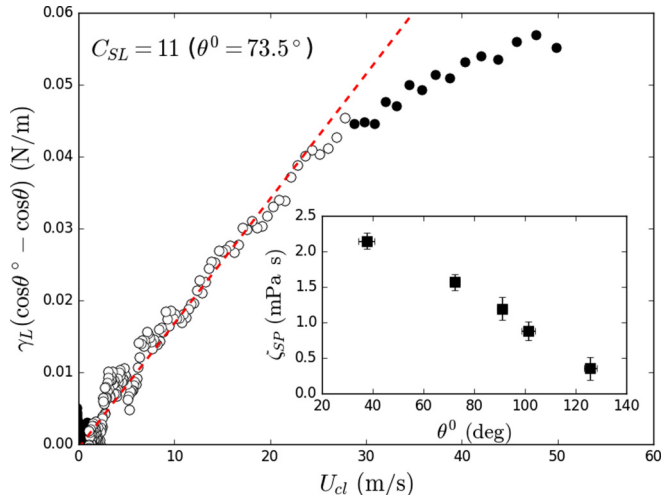


FIG. 4. Spreading drop simulations. The main chart shows the capillary driving force $\gamma_L(\cos\theta^0 - \cos\theta_D)$ plotted vs contact-line velocity U_{cl} for coupling $C_{SL} = 11$. The dashed line is the fit to Eq. (2) (open symbols). The inset shows the contact-line friction ζ_{SP} for all couplings studied vs the corresponding equilibrium contact angle.

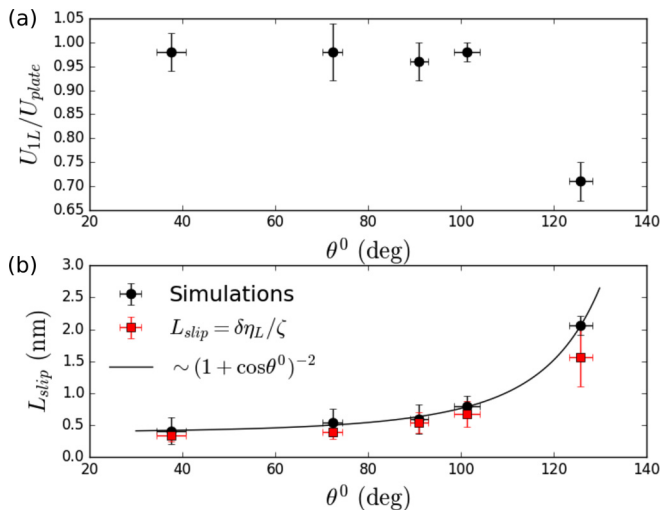


FIG. 5. (a) Ratio of U_{1L}/U_{plate} and (b) the slip length L_{slip} for simulations of a liquid bridge between moving plates. Both are plotted vs the equilibrium contact angle. Also plotted in (b) are the slip lengths obtained using Eq. (8), with $\delta = 1.06$ nm, $\eta_L = 0.64$ mPa s, and averaged values of ζ from Table I. The solid line is the correlation proposed by Huang *et al.* [45].

shows a typical plot of the capillary driving force versus the contact-line velocity for $C_{SL} = 11$. At sufficiently low contact-line velocities there is a clearly linear relation between F_{cl} and U_{cl} , in agreement with Eq. (2), from which we may extract the coefficient of contact-line friction ζ_{SP} and its error by simple linear regression. The values of ζ_{SP} for all the solid-liquid couplings studied and the corresponding equilibrium contact angles are listed in Table I and plotted in the inset in Fig. 4. The data in Fig. 4 do show nonlinearity at the highest velocities, and if one fits all the data shown with Eq. (1), one recovers almost exactly the same value for ζ_{SP} as from the linear fit. However, it is possible that the nonlinearity is due, at least in part, to the uncertainties surrounding the early stages of contact between the liquid drop and the solid, as discussed in Sec. III B. Therefore we have chosen not to take this approach until we can be more certain of the significance of the high-velocity data.

B. Forced wetting of liquid bridge

Snapshots of the change in the shape of the liquid bridge as U_{plate} is increased from zero to 24 m/s for $C_{SL} = 9$ are illustrated in Figs. 1(d)–1(f). In order to investigate the significance of slip in our simulations, we determine the velocity of the liquid in contact with the plates as follows. The system is symmetrical in the y direction; hence all the liquid atoms may be projected onto the x - z plane, which we subdivide into a grid of squared bins of 0.5 nm side. First we compute the average velocity of the atoms in the x and z direction within each bin every 10^3 time steps. We then average the velocities over 500 saved snapshots to further reduce noise and determine the standard deviation. This allows us to obtain the mean velocity of the atoms in each cell and measure the velocity gradient du_x/dz in the center of the liquid, well away from the contact lines. Finally, from the velocity gradient at its intersection with the plates we compute the velocity of the liquid in contact with the plates U_{1L} .

Figure 5 shows the ratio U_{1L}/U_{plate} and the slip length L_{slip} (the distance into the solid at which the linearly extrapolated fluid velocity vanishes) for each solid-liquid coupling; $L_{slip} = 0$ corresponds to no slip. The slip lengths are also listed in Table I. Clearly, there is significant slip at low couplings, but this becomes almost negligible, within the uncertainty, for $C_{SL} = 8$, suggesting that slip tends

to a constant low value below a contact angle of about 90 deg. Based on this data, slip for water is significantly less than we found for a very similar substrate with L-J liquids [21]. In this study we found slip to be an exponentially decreasing function of the work of adhesion $Wa^0 = \gamma_L(1 + \cos \theta^0)$. But even without a formal link with Wa^0 , it seems self-evident that for a partially wetting system, low slip requires a strong solid-liquid attraction combined with a high surface tension. Hence, the principle reason for the reduction in slip is probably the much higher surface tension of the simulated water: 56.8 mN/m compared with 2.49 mN/m for the L-J fluids.

Experimental studies of the dynamic contact angle of water on partially wetting substrates are rare and do not usually cover a sufficiently wide range of speeds to extract reliable values of ζ . However, one study of water wetting poly(ethylene terephthalate) (PET) at speeds up to 10 m/s has been reported [25], which allows one to calculate a value of $\zeta = 11.8$ mPa s. This is about 7 times higher than that found for $C_{SL} = 11$, which yields a static contact angle of 72 deg, close to the experimental value for water on PET. Presumably, the difference in ζ is due primarily to the different structure and composition of the molecularly smooth, carbonlike surface used in our simulations and the PET surface, which, though specularly reflecting, is rough and heterogeneous at the nanoscale [44]. More work is required to verify this or provide an alternative explanation.

In Ref. [21] we proposed a direct link between the coefficients of slip and contact-line friction, $\beta = \zeta/\delta$, where δ is the width of the three-phase zone and $\beta = \eta_L/L_{\text{slip}}$, i.e., we assume a linear Navier slip condition. This leads to

$$L_{\text{slip}} = \delta\eta_L/\zeta. \quad (8)$$

We can estimate δ from the distance over which the density of the first layer of liquid in contact with the solid decays to zero at the contact line. For $C_{SL} = 9$ ($\theta^0 = 90$ deg), $\delta = 1.06$ nm. The resulting values of L_{slip} predicted by Eq. (8) are plotted in Fig. 5(b) for $\eta_L = 0.64$ mPa s [42] and the average value of ζ at each coupling. The agreement with the slip lengths measured directly from the velocity gradients is excellent and would seem to confirm that contact-line friction and slip share a common mechanism, namely, the interaction of the liquid molecules with the energy landscape of the solid surface. Using scaling arguments, Huang *et al.* [45] have proposed that L_{slip} is related to θ^0 by $L_{\text{slip}} \sim (1 + \cos \theta^0)^{-2}$. This is shown by the solid line in Fig. 5(b) and is supported by our data.

Figure 6 shows the driving force $\gamma_L(\cos \theta^0 - \cos \theta_D)$ plotted versus the slip-corrected value of the contact-line velocity U_{cl} for each solid-liquid coupling. Since $U_{cl} = U_{cl}^{\text{app}} - U_{\text{slip}}$ and $U_{cl}^{\text{app}} = -U_{\text{plate}}$, it follows that $U_{cl} = -(U_{\text{plate}} + U_{\text{slip}})$. As all the plots are linear, we can determine the contact-line friction ζ_{MP} directly from the slopes using Eq. (3). The resulting values are listed in Table I and plotted versus the corresponding equilibrium contact angle in the inset in Fig. 6.

C. Contact-line fluctuations

To study the fluctuations of the contact line at each solid-liquid coupling, we start from an equilibrium configuration of a capillary bridge with its four contact lines, such as that depicted in Fig. 1(d), and monitor the simulation for an additional 2×10^6 time steps (4 ns). To determine the locations of the contact lines, we first select a slice of liquid in the x - y plane adjacent to each S-L interface and determine the density profile in the z direction. The density is constant in the bulk but becomes layered in proximity to the plates. We define the first layer of liquid as the slice containing the first peak in the density profile. We save the averaged density profiles of this first layer in the x direction every 10 time steps. Each saved density profile is constant across the majority of the S-L interface but decays to zero at each contact line. We define the contact-line position $x_{cl}(t)$ at time t as the value of x at which the density profile decays to 50% of its central value.

Once we have located the position of the contact line at each time step, we compute its mean location x_{cl}^0 and subtract it from its instantaneous position to determine the probability density function (PDF) of $\Delta x(t) = x_{cl}(t) - x_{cl}^0$. The results for all five couplings studied are plotted in Fig. 7. Each distribution can be fitted by a Gaussian function with a mean value of zero and a standard deviation σ equal to half the width of the distribution between the two inflection points.

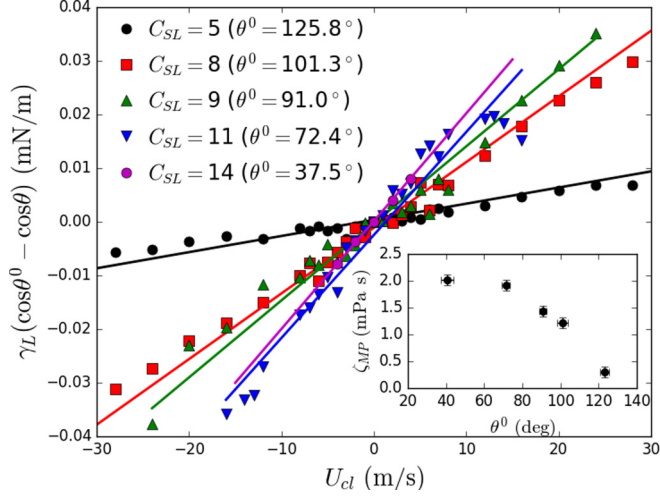


FIG. 6. Forced wetting of a liquid bridge between moving plates. The main chart shows the capillary driving force $\gamma_L(\cos\theta^0 - \cos\theta)$ plotted vs the contact-line velocity $U_{cl} = -(U_{plate} + U_{slip})$ for each coupling C_{SL} studied. The inset shows the corresponding coefficients of contact-line friction ζ_{MP} vs the equilibrium contact angle.

We can then compute the values of $\sigma^2 L_y$ for the different solid-liquid couplings and equilibrium contact angles. These values are listed in Table I and plotted in the inset in Fig. 7. The error bars are computed as the standard deviation of the $\sigma^2 L_y$ parameters measured at the four contact lines. As can be seen, the amplitude of the contact-line fluctuations, $\sigma^2 L_y$, is insensitive to the coupling and, within the error bars, tends to a constant value above $C_{SL} = 8$, which corresponds to contact angles below 90 deg. Significantly, this is the same threshold below which slip becomes very small.

Figure 8 depicts an example of the decay of the self-correlation function normalized by the variance of the contact-line position $\langle x_{cl}(t + t_0)x_{cl}(t_0) \rangle_{t_0} / \sigma^2$ for the lowest coupling studied,

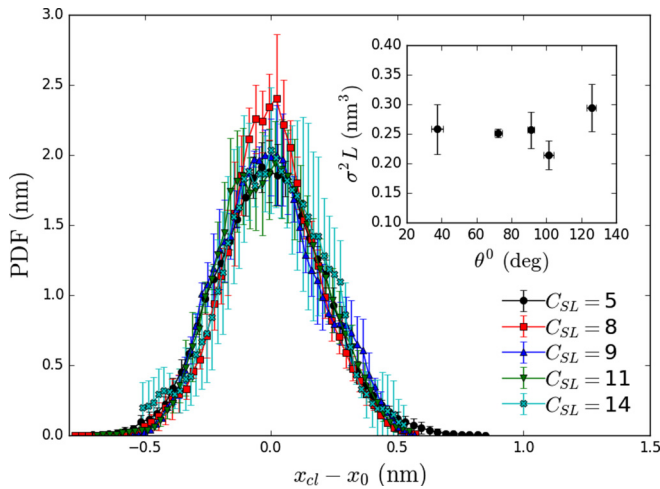


FIG. 7. Probability density function (PDF) of the contact-line position about its mean location computed from the Gaussian fits (lines) to the density histograms (symbols) for a contact line of length $\Delta y = L_y$ and solid-liquid couplings $C_{SL} \in [5, 14]$. Inset: Computed $\sigma^2 L_y$ parameters vs the average equilibrium contact angle.

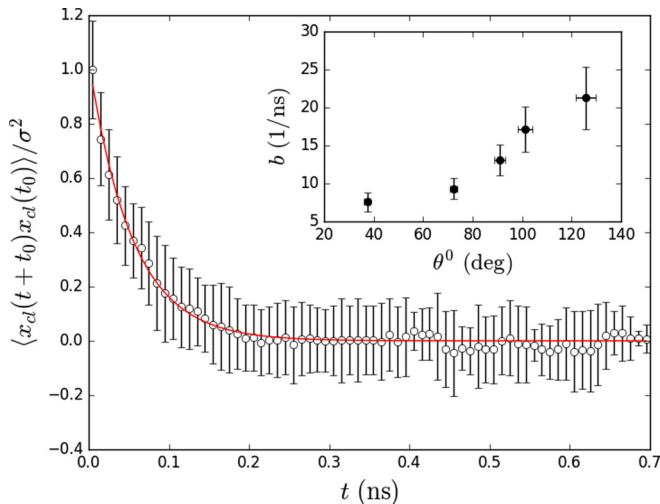


FIG. 8. Normalized self-correlation function $\langle x_{cl}(t+t_0)x_{cl}(t_0) \rangle_{t_0} / \sigma^2$ vs time t for $C_{SL} = 5$ and the fit to Eq. (6). Inset: Decay parameter b vs the average equilibrium contact angle.

$C_{SL} = 5$. The line through the data is the best fit to Eq. (6), which yields the decay parameter b . The values of b found for each coupling are listed in Table I and plotted versus the equilibrium contact angle in the inset of Fig. 8. The error bars represent the standard deviation of b measured at the four contact lines. Now that we have both $\sigma^2 L_y$ and b , the coefficients of contact-line friction, ζ_F , can be obtained from the fluctuations via Eq. (7). The resulting values are also shown in Table I.

It is interesting that unlike the amplitude of the fluctuations, the correlation decay parameter b (the units of which are frequency) decreases continuously as the coupling is increased. Given that the fluctuations of the contact line must reflect the collective behavior of the atoms that comprise it, both trends are consistent with the MKT. While the characteristic distance of individual molecular displacements within the three-phase zone, λ , tends to have a fixed value for a given system, assumed to be related to the distribution of S-L interaction sites (the potential energy wells in our simulation), both experiment and simulation confirm that the characteristic frequency of the displacements κ^0 decreases continuously with the increasing S-L interaction and therefore with decreasing θ^0 [28].

V. DISCUSSION

Our paper has focused on the use of MD simulations to determine the coefficients of contact-line friction of a waterlike liquid on a molecularly smooth carbonlike solid surface. We have taken two different approaches. The first involved dynamic contact angle measurements during both spontaneous spreading and forced steady wetting. The second was based on a Langevin treatment of the fluctuations of a contact line at *equilibrium*. The results are compared in Fig. 9. Both approaches yield values that are compatible within the probable errors. This is convincing evidence that both measure the same thing and that the concept of contact-line friction is well founded and capable of being extended to explore a broad range of wetting problems.

Contact-line friction is an essentially simple concept, not unlike the Navier slip condition. The proposition is that for a contact line to move at a velocity U_{cl} , a force F_{cl} must be applied proportional to the velocity to overcome resistance to motion along the solid surface, i.e., $F_{cl} = \zeta U_{cl}$. The prefactor ζ contains no details regarding its origin. It arose, initially, as the linear, low-speed limit of the molecular-kinetic theory of dynamic wetting discussed in Sec. II A, in which F_{cl} is identified with the out-of-balance capillary force $\gamma_L(\cos \theta^0 - \cos \theta_D)$ that arises when the contact

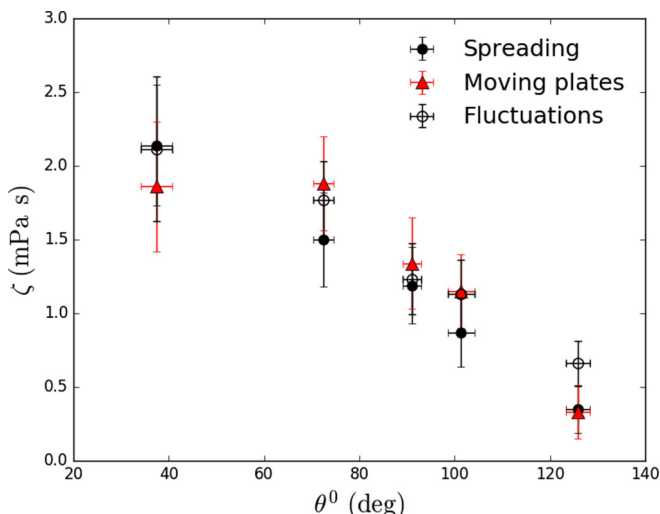


FIG. 9. Comparison of the contact-line friction coefficients measured by our three different simulation methods vs the equilibrium contact angle θ^0 : spontaneous spreading ζ_{SP} , moving plates ζ_{MP} , and fluctuations ζ_F .

angle deviates from its equilibrium value. As envisaged at its inception [46], the MKT encompasses all dissipative events at the contact line that are susceptible to Maxwell-Boltzmann statistics. Thus κ^0 and λ are effective quantities, not necessarily linked to one type of event. As such, it has proved effective in describing dynamic wetting in both experiment and simulations.

However, the existence of contact-line friction is not necessarily tied to this explanation. Equation (2), used to fit our dynamic contact angle data to obtain ζ , contains no molecular information, and, as we have shown here and previously [22], one can measure ζ simply from the damping of contact-line fluctuations, without any reference to a particular molecular model. Thus it is very general. For example, in addition to solid-liquid interactions at the level of individual molecules, contact-line friction may also occur as a result of microscopic pinning or depinning events on rough or heterogeneous surfaces [47–49]. More collective events such as these would have a natural influence on the fluctuations and so would be reflected in the values of $\sigma^2 L_y$ and b , and hence in ζ . The individual events would go unnoticed in experiments until the scale was sufficient to cause contact angle hysteresis. Furthermore, in many practical systems other factors such as insoluble surfactants, colloidal particles, complex rheological effects, or local viscoelastic deformation of soft substrates might well play a part.

Despite this range of possibilities, the idea that the low-speed regime of dynamic wetting can be described by a unique prefactor ζ retains within it the powerful idea that the contact region, however one wishes to model it, is a special place with special properties, which cannot move across a solid surface without incurring energy loss. Moreover, the Langevin treatment of the contact-line fluctuations proves that contact-line friction is a function of only the equilibrium properties of the system. The fluctuations are just the collective result of the thermal motion of the constituent molecules, and the damping friction they experience arises simply because of their interaction with the energy landscape of the solid surface.

Our studies have also confirmed the close relationship between contact-line friction and slip at the solid-liquid interface far away from the contact line. Both appear to be linked by a common molecular mechanism, as demonstrated in Fig. 5(b) by the close agreement between the measured and predicted slip lengths. Interestingly, the full sinh form of Eq. (1) has been shown to account very well for the nonlinear dependence of slip length on shear stress found in MD simulation of simple liquids on smooth solids [50–52]. Convincing evidence of the nonlinearity predicted by Eq. (1) has

not yet been reported for dynamic contact angle simulations, but in none of the model systems so far studied has the argument in the sinh function of Eq. (1), $\gamma_L \lambda^2 / k_B T$, significantly exceeded unity. However, the success of the sinh relationship for slip at very high shear stresses is encouraging.

The clear link between contact-line friction and slip serves to emphasize that Eq. (2) may be regarded as a Navier slip boundary condition specific to the contact line [25,53–56]. This boundary condition contains not only the required length and energy scales defining slip but also yields the necessary geometric boundary condition, namely, the local, microscopic contact angle. As such, it could reasonably be integrated within the continuum hydrodynamic model [56]. Indeed, a recent multiscale study of droplet spreading has combined the MKT with both MD and computational fluid mechanics with considerable success [57]. Similarly, a contact-line friction model based on the general slip model of Thompson and Troian has been successfully used in combination with computational fluid mechanics. The results compare favorably with MD simulations [58]. In the same spirit, diffuse interface treatments of the moving contact line have been combined with numerical modeling to reproduce results that align with MD studies. This has led to a generalization of the Navier slip boundary condition to include the stress inside the diffuse interface (the GNBC) [59–62]. Slip at the contact line is then proportional to the sum of the tangential viscous stress and the uncompensated surface tension stress arising from the deviation in the microscopic contact angle from its equilibrium value. Thus it seems that our understanding of dynamic wetting is gradually converging to a more unified view. Ultimately, however, the goal must be to incorporate the stochastic nature of the moving contact line into continuum mechanics. A move in this direction has been made by Perrin *et al.*, who used a Langevin description of contact-line motion over nanoscale defects to construct a multiscale model of dynamic wetting [49].

Finally, we note that the simple linear relationship between force and velocity has potentially wide applications to wetting processes in nanotechnology, where speeds are likely to be small. For example, it has recently been applied to the movement of nanodrops across a solid surface [63]. Here the simulations showed that the same coefficient of contact-line friction could be used to predict the dynamic contact angle at all points around the liquid drop. It is also worth pointing out that ζ is demonstrably proportional to viscosity [28]; hence we may also write an equivalent linear relationship between the capillary number $Ca = U_{cl} \eta_L / \gamma_L$ and a dimensionless driving force $(\cos \theta^0 - \cos \theta_D)$ [25,56].

VI. CONCLUSIONS

Previous molecular-dynamics investigations of dynamic wetting have, for reasons of computational economy, usually involved rather simple Lennard-Jones solids and liquids [5–9,20,21,60,64]. Useful insight has been gained regarding the behavior of the local microscopic contact angle and related phenomena such as slip between liquids and solids. However, questions remain regarding the generality of the findings when translated to real systems with more complicated structures and potentials.

To begin to address these questions, we have used large-scale MD simulations to investigate the velocity dependence of the dynamic contact angle of a waterlike liquid on a flat carbonlike solid surface. Two configurations have been studied: a liquid drop spreading spontaneously on a stationary solid surface and a liquid bridge in Couette flow between two solid surfaces moving in opposite directions at a range of steady speeds. To determine the influence of the intrinsic wettability of the solid surface, we have systematically varied the solid-liquid attraction, yielding a range of equilibrium contact angles from 38 to 126 deg. The resulting dynamic contact angle behavior was found to fall into the linear region governed by Eq. (2), $\zeta U_{cl} = \gamma_L (\cos \theta^0 - \cos \theta_D)$, from which we extracted the relevant coefficients of contact-line friction ζ , which characterize the frictional losses when the contact line moves across a solid surface. Perhaps more significantly, we have extended very recent work with L-J liquids [22] to the water system and applied a Langevin formalism to extract the coefficients of contact-line friction directly from the equilibrium fluctuations of the contact line, without any additional theoretical interpretation or model.

The principle conclusion to be drawn from all these different studies using a realistic liquid simulation is that all three methods measure the same quantity. All three yield values for the coefficient of contact-line friction that are compatible within the probable errors. Taken together, our results show that the linear regime of dynamic wetting can be described by a unique prefactor ζ that is a function of only the equilibrium properties of the system. Contact-line friction is a real phenomenon that must be accommodated by any complete theory of dynamic wetting [65]. Thus our general approach to dynamic wetting is consistent and capable of being used to expand our understanding and explore a broad range of practical wetting problems. These include problems encountered in areas such as nanotechnology, where the concept of a linear relationship between driving force and velocity may provide a very useful simplification.

Another finding from our study is that slip between water and a molecularly flat, partially wetted solid surface is minimal, with slip lengths of little more than the diameter of a water molecule for equilibrium contact angles of 90 deg or less. Furthermore, we have confirmed a mechanistic link between the coefficients of slip and contact-line friction. This means that measurements of the dynamic contact angle or contact-line fluctuations may potentially be used to predict slip and vice versa. It also opens the way to a more unified hydrodynamic treatment.

In future work we hope to extend these studies to more complex surfaces and explore whether or not it is possible with MD simulations to demonstrate the nonlinearity predicted by Eq. (1) and readily seen in experiments. Another goal is to measure both the microscopic and apparent dynamic contact angles in a single simulation. This could illuminate the crossover between thermally activated wetting and hydrodynamics.

ACKNOWLEDGMENTS

The authors thank the European Space Agency (ESA) under Grant No. AO-2004-096 and the Belgian Federal Science Policy (BELSPO) for their support within the framework of the PRODEX program. M.K. acknowledges financial support from the Slovenian Research Agency (Research Core Funding No. P1-0055 and Research Grant No. J1-1701). Computational resources have been provided by the Consortium des Equipements de Calcul Intensif (CECI), funded by the Fonds de la Recherche Scientifique de Belgique (F.R.S.-FNRS) under Grant No. 2.5020.11.

-
- [1] L. Chen, J. Yu, and H. Wang, Convex nanobending at a moving contact line: The missing mesoscopic link in dynamic wetting, *ACS Nano* **8**, 11493 (2014).
 - [2] S. Guo, M. Gao, X. Xiong, Y. J. Wang, X. Wang, P. Sheng, and P. Tong, Direct Measurement of Friction of a Fluctuating Contact Line, *Phys. Rev. Lett.* **111**, 026101 (2013).
 - [3] M. Engel, P. W. Bryant, R. F. Neumann, R. Giro, C. Feger, P. Avouris, and M. Steiner, A platform for analysis of nanoscale liquids with an array of sensor devices based on two-dimensional material, *Nano Lett.* **17**, 2741 (2017).
 - [4] G. Chen, H. H. Bau, and C. H. Li, In situ transmission electron microscope liquid cell 3D profile reconstruction and analysis of nanoscale liquid water contact line movements, *Langmuir* **35**, 16712 (2019).
 - [5] J. Koplik, J. R. Banavar, and J. F. Willemsen, Molecular dynamics of fluid flow at solid surfaces, *Phys. Fluids A* **1**, 781 (1989).
 - [6] P. A. Thompson and M. O. Robbins, Simulations of Contact-Line Motion: Slip and the Dynamic Contact Angle, *Phys. Rev. Lett.* **63**, 766 (1989).
 - [7] M. J. de Ruijter, T. D. Blake, and J. De Coninck, Dynamic wetting studied by molecular modeling simulations of droplet spreading, *Langmuir* **15**, 7836 (1999).
 - [8] D. R. Heine, G. S. Grest, and E. B. Webb, Spreading dynamics of polymer nanodroplets in cylindrical geometries, *Phys. Rev. E* **70**, 011606 (2004).

- [9] J. De Coninck and T. Blake, Wetting and molecular dynamics simulations of simple liquids, *Annu. Rev. Mater. Res.* **38**, 1 (2008).
- [10] P. A. Thompson and S. M. Troian, A general boundary condition for liquid flow at solid surfaces, *Nature (London)* **389**, 360 (1997).
- [11] N. V. Priezjev and S. M. Troian, Molecular Origin and Dynamic Behavior of Slip in Sheared Polymer Films, *Phys. Rev. Lett.* **92**, 018302 (2004).
- [12] E. Lauga, M. Brenner, and H. Stone, Microfluidics: The no-slip boundary condition, in *Springer Handbook of Experimental Fluid Mechanics* (Springer, Berlin, 2007), pp. 1219–1240.
- [13] D. Sergi, G. Scocchi, and A. Ortona, Molecular dynamics simulations of the contact angle between water droplets and graphite surfaces, *Fluid Phase Equilib.* **332**, 173 (2012); Note: These authors used the same values of ϵCO and aOS as in our simulations, but their substrate was graphite, which has a different structure to our solid, and so they obtained a different equilibrium contact angle with $CSL = 1$.
- [14] L. Zhao and J. Cheng, Analyzing the molecular kinetics of water spreading on hydrophobic surfaces via molecular dynamics simulation, *Sci. Rep.* **7**, 10880 (2017).
- [15] M. Haratsuka, M. Emoto, A. Konno, and S. Ito, Molecular dynamics simulation of the influence of nanoscale structure on water wetting and condensation, *Micromachines* **10**, 587 (2019).
- [16] J. Yan, G. Liu, T. Wang, J. Zhao, Y. Ding, and N. Chen, Analysis of superhydrophobic material performance based on molecular dynamics simulations, *Surf. Eng.* **32**, 147 (2016).
- [17] H. Li and K. Zhang, Dynamic behavior of water droplets impacting on superhydrophobic surfaces: Both experimental study and molecular dynamics simulation study, *Appl. Surf. Sci.* **498**, 143793 (2019).
- [18] K. Falk, F. Sedlmeier, L. Joly, R. Netz, and L. Bocquet, Molecular origin of fast water transport in carbon nanotube membranes: Superlubricity versus curvature dependent friction, *Nano Lett.* **10**, 4067 (2010).
- [19] S. Xiao, J. He, and Z. Zhang, Nanoscale deicing by molecular dynamics simulation, *Nanoscale* **8**, 14625 (2016).
- [20] E. Bertrand, T. D. Blake, and J. De Coninck, Influence of solid-liquid interactions on dynamic wetting: A molecular dynamics study, *J. Phys.: Condens. Matter* **21**, 464124 (2009).
- [21] T. D. Blake, J.-C. Fernández-Toledano, G. Doyen, and J. De Coninck, Forced wetting and hydrodynamic assist, *Phys. Fluids.* **27**, 112101 (2015).
- [22] J.-C. Fernández-Toledano, T. D. Blake, and J. De Coninck, Contact-line fluctuations and dynamic wetting, *J. Colloid Interface Sci.* **540**, 322 (2019).
- [23] J.-C. Fernández-Toledano, T. D. Blake, and J. De Coninck, Moving contact lines and Langevin formalism, *J. Colloid Interface Sci.* **562**, 287 (2019).
- [24] T. D. Blake and J. M. Haynes, Kinetics of liquid/liquid displacement, *J. Colloid Interface Sci.* **30**, 421 (1969).
- [25] T. D. Blake, Dynamic contact angles and wetting kinetics, in *Wettability* (Marcel Dekker, New York, 1993), pp. 252–309.
- [26] T. D. Blake and J. De Coninck, The influence of solid-liquid interactions on dynamic wetting, *Adv. Colloid Interface Sci.* **96**, 21 (2002).
- [27] T. D. Blake, The physics of moving wetting lines, *J. Colloid Interface Sci.* **299**, 1 (2006).
- [28] D. Duvivier, T. D. Blake, and J. De Coninck, Toward a predictive theory of wetting dynamics, *Langmuir* **29**, 10132 (2013).
- [29] N. V. Priezjev, Effect of surface roughness on rate-dependent slip in simple fluids, *J. Chem. Phys.* **127**, 144708 (2007).
- [30] C. Huh and L. E. Scriven, Hydrodynamic model of steady movement of a solid/liquid/fluid contact line, *J. Colloid Interface Sci.* **35**, 85 (1971).
- [31] P. Langevin, On the theory of Brownian motion, *C. R. Acad. Sci. Paris* **146**, 530 (1908).
- [32] M. Doi and S. Edwards, *The Theory of Polymer Dynamics* (Oxford University Press, Oxford, England, 1986).
- [33] S. Plimpton, Fast parallel algorithms for short-range molecular dynamics, *J. Comput. Phys.* **117**, 1 (1995).
- [34] T. Werder, J. H. Walther, R. L. Jaffe, T. Halicioglu, F. Noca, and P. Koumoutsakos, Molecular dynamics simulation of contact angles of water droplets in carbon nanotubes, *Nano Lett.* **1**, 697 (2001).

- [35] M. Khalkhali, N. Kazemi, H. Zhang, and Q. Liu, Wetting at the nanoscale: A molecular-dynamics study, *J. Chem. Phys.* **146**, 114704 (2017).
- [36] B. A. Noble, C. M. Mate, and B. Raeymaekers, Spreading kinetics of ultrathin liquid films using molecular dynamics, *Langmuir* **33**, 3476 (2017).
- [37] M. P. Allen and D. J. Tildesley, *Computer Simulation of Liquids* (Clarendon Press, New York, 1989).
- [38] H. J. C. Berendsen, J. R. Grigera, and T. P. Straatsma, The missing term in effective pair potentials, *J. Phys. Chem.* **91**, 6269 (1987).
- [39] H. C. Andersen, RATTLE: A “Velocity” version of the SHAKE algorithm for molecular dynamics calculations, *J. Comput. Phys.* **52**, 24 (1983).
- [40] J. P. R. B. Walton, D. J. Tildesley, J. S. Rowlinson, and J. R. Henderson, The pressure tensor at the planar surface of a liquid, *Mol. Phys.* **48**, 1357 (1983).
- [41] C. Vega and E. de Miguel, Surface tension of the most popular models of water by using the test-area simulation method, *J. Chem. Phys.* **126**, 154707 (2007).
- [42] S. Tazi, A. Botan, M. Salanne, V. Marry, P. Turq, and B. Rotenberg, Diffusion coefficient and shear viscosity of rigid water models, *J. Phys.: Condens. Matter* **24**, 284117 (2012).
- [43] S. Perumanath, M. K. Borg, M. V. Chubynsky, J. E. Sprittles, and J. M. Reese, Droplet Coalescence is Initiated by Thermal Motion, *Phys. Rev. Lett.* **122**, 104501 (2019).
- [44] T. D. Blake and G. N. Batts, The temperature dependence of the dynamic contact angle, *J. Colloid Interface Sci.* **553**, 108 (2019).
- [45] D. M. Huang, C. Sendner, D. Horinek, R. R. Netz, and L. Bocquet, Water Slippage Versus Contact Angle: A Quasiuniversal Relationship, *Phys. Rev. Lett.* **101**, 226101 (2008).
- [46] T. D. Blake, The contact angle and two-phase flow, Ph.D. thesis, Bristol University, 1968.
- [47] K. Davitt, M. S. Petterson, and E. Rolley, Thermally activated wetting dynamics in the presence of surface roughness, *Langmuir* **29**, 6884 (2013).
- [48] M. Ramiasa, J. Ralston, R. Fetzer, R. Sedev, D. M. Fopp-Spori, C. Morhard, C. Pacholski, and J. P. Spatz, Contact-line motion on nanorough surfaces: A thermally activated process, *J. Am. Chem. Soc.* **135**, 7159 (2013).
- [49] H. Perrin, R. Lhermerout, K. Davitt, E. Rolley, and B. Andreotti, Defects at the Nanoscale Impact Contact Line Motion at All Scales, *Phys. Rev. Lett.* **116**, 184502 (2016).
- [50] F. Yang, Slip boundary condition for viscous flow over solid surfaces, *Chem. Eng. Commun.* **197**, 544 (2010).
- [51] H. Hu, L. Bao, N. Priezjev, and K. Luo, Identifying two regimes of slip of simple fluids over smooth solid surfaces with weak and strong wall-fluid interaction energies, *J. Chem. Phys.* **146**, 034701 (2017).
- [52] G. J. Wang and N. Hadjiconstantinou, Universal molecular-kinetic scaling relation for slip of a simple fluid at a solid boundary, *Phys. Rev. Fluids* **4**, 064201 (2019).
- [53] J. E. Ruckenstein and C. S. Dunn, Slip velocity during wetting of solids, *J. Colloid Interface Sci.* **59**, 135 (1977).
- [54] P. Neogi and C. A. Miller, Spreading kinetics of a drop on a smooth solid surface, *J. Colloid Interface Sci.* **86**, 525 (1982).
- [55] W. Ren, D. Hu, and E. Weinan, Continuum models for the contact line problem, *Phys. Fluids* **22**, 102103 (2010).
- [56] J. H. Snoeijer and B. Andreotti, Moving contact lines: Scales, regimes, and dynamical transitions, *Annu. Rev. Fluid Mech.* **45**, 269 (2013).
- [57] J. Zhang, M. K. Borg, and J. M. Reese, Multiscale simulation of dynamic wetting, *Int. J. Heat Mass Transfer* **115**, 886 (2017).
- [58] A. V. Lukyanov and T. Pryer, Hydrodynamics of moving contact lines: Macroscopic versus microscopic, *Langmuir* **33**, 8582 (2017).
- [59] T. Qian, X.-P. Wang, and P. Sheng, Molecular scale contact line hydrodynamics of immiscible flows, *Phys. Rev. E* **68**, 016306 (2003).
- [60] T. Qian, X.-P. Wang, and P. Sheng, A variational approach to the moving contact line hydrodynamics, *J. Fluid Mech.* **564**, 333 (2006).

- [61] A. Carlson, M. Do-Quang, and G. Amberg, Dissipation in rapid dynamic wetting, *J. Fluid Mech.* **682**, 213 (2011).
- [62] W. Ren and E. Weinan, Boundary conditions for the moving contact line problem, *Phys. Fluids* **19**, 022101 (2007).
- [63] J.-C. Fernández-Toledano, T. D. Blake, L. Limat, and J. De Coninck, A molecular-dynamics study of sliding liquid nanodrops: Dynamic contact angles and the pearling transition, *J. Colloid Interface Sci.* **548**, 66 (2019).
- [64] A. V. Lukyanov and A. E. Likhtman, Dynamic contact angle at the nanoscale: A unified view, *ACS Nano* **10**, 6045 (2016).
- [65] A. Carlson, G. Bellani, and G. Amberg, Universality in dynamic wetting dominated by contact-line friction, *Phys. Rev. E* **85**, 045302(R) (2012).